Nanoscale Res Lett (2010) 5:735–740
DOI 10.1007/s11671-010-9547-8

NANO EXPRESS

# Morphological and Electrochemical Properties of Crystalline Praseodymium Oxide Nanorods

**M. Shamshi Hassan · M. Shaheer Akhtar · Kyung-Bo Shim · O-Bong Yang**

Received: 24 August 2009 / Accepted: 17 January 2010 / Published online: 5 February 2010


**Abstract** Highly crystalline $Pr_6O_{11}$ nanorods were prepared by a simple precipitation method of triethylamine complex at 500°C. Synthesized $Pr_6O_{11}$ nanorods were uniformly grown with the diameter of 12–15 nm and the length of 100–150 nm without any impurities of unstable $PrO_2$ phase. The $Pr_6O_{11}$ nanorod electrodes attained a high electrical conductivity of 0.954 $Scm^{-1}$ with low activation energy of 0.594 eV at 850°C. The electrochemical impedance study showed that the resistance of electrode was significantly decreased at high temperature, which resulted from its high conductivity and low activation energy. The reduced impedance and high electrical conductivity of $Pr_6O_{11}$ nanorod electrodes are attributed to the reduction of grain boundaries and high space charge width.

**Keywords** Praseodymium oxide · Nanorods · Impedance spectroscopy · Electrochemical property

## Introduction

The crystalline praseodymium oxide (PrOx) is a promising material for many potential applications in nanodevices and microelectronics devices due to its high-K dielectric with an effective dielectric constant of around 30 and very low leakage currents [1]. Praseodymium oxides have been used as high electrical conductive materials [2], a semiconducting oxide for dielectric materials [3], sensing materials for detection of ethanol vapor [4], organic light-emitting diode [5], oxygen-storage components of three-way automotive catalysts [6] and non-volatile ferroelectric random access memory (Nv-FRAM) devices [7]. Among PrOx such as $PrO_2$, $Pr_2O_3$ and $Pr_6O_{11}$, $Pr_6O_{11}$ shows exceptionally high electrical conductivity due to electron hopping between the mixed metal ion valence states of the lattice [8].

It was reported that $Pr_6O_{11}$ nanotubes and nanorods were synthesized by a molten salt method [9] and a hydrothermal method [10], respectively. The morphological properties of $Pr_6O_{11}$ nanomaterials were reported in literature [2, 11]. However, there are few reports on electrochemical properties such as conductivity and impedance of the praseodymium oxide nanomaterials, even though these materials are having advanced morphological and crystalline properties. In this paper, we report the electrochemical properties as well as morphological properties of the synthesized polycrystalline $Pr_6O_{11}$ nanorods by a simple precipitation method.

## Experimental

### Synthesis of $Pr_6O_{11}$ Nanorods

In a typical synthesis, 2 g of $Pr(NO_3)_3{\cdot}6H_2O$ powder (purity 99.5%, Sigma–Aldrich chemicals) was dissolved in a mixture of isopropanol and cyclohexane with the ratio of 1:4 and stirred until the solution become transparent. Triethylamine was added in the reaction mixture as complexing agent. The white precipitate was formed after a few minutes. The obtained precipitate was filtered and washed with distilled and deionized water and dried at 80°C in air. The crude synthesized powder was calcined at 500°C for 2 h in an ambient condition to produce $Pr_6O_{11}$ nanorods.

M. Shamshi Hassan · M. Shaheer Akhtar · K.-B. Shim · O.-B. Yang (✉)
School of Semiconductor and Chemical Engineering and Solar Energy Research Center, Chonbuk National University, Jeonju 561-756, Republic of Korea
e-mail: obyang@jbnu.ac.kr

## Characterizations

Electrochemical impedance spectroscopy (EIS) was taken with the thin film electrode of $Pr_6O_{11}$ coated on fluorine-doped tin oxide glass (FTO, Hartford Glass Co., 8 Ω/sq, 80% transmittance). For the preparation of $Pr_6O_{11}$ nanorods films, $Pr_6O_{11}$ nanorods slurry was prepared using aqueous polyethylene glycol (Fluka, MW 20,000) solution under vigorous grinding. Thus, prepared uniform slurry was coated on FTO glass with a thickness of about 10 μm and active area of $\sim 0.5 \times 0.5$ cm$^2$ by a doctor blade technique. The film was calcined at 400°C for 1 h. To fabricate an electrochemical cell, a Pt counter electrode glass was placed over the $Pr_6O_{11}$ electrode and the edges of the cell were sealed with 60-μm-thick sealing sheet (SX 1170-60, Solaronix) by pressing the two electrodes together on a double hot-plate at 70°C. Finally, an electrolyte of LiI (0.5 M) and $I_2$ (0.05 M) in acetonitrile was introduced into the cell through one of two small holes drilled in the counter electrode. EIS measurement of fabricated $Pr_6O_{11}$ electrochemical cells was performed using an AC impedance analyzer (VersaSTAT 4) in the frequency range from 10 to 1 MHz with signal amplitude of 10 mV. Electrical conductivity of $Pr_6O_{11}$ nanorods material was measured in air by four-probe DC method in the temperature range of 20–850°C. $Pr_6O_{11}$ nanorod powder was pressed into cylindrical pallet and then calcined at 1,000°C for 5 h.

## Results and Discussion

Figure 1 shows the low and high magnification field emission scanning electron microscopy (FESEM, Hitachi 4700) images of synthesized $Pr_6O_{11}$ nanorods. The $Pr_6O_{11}$ nanorods were uniform and well grown with 12–15 nm diameter and 100–150 nm length. The energy-dispersive X-ray spectroscopy (EDX) analysis was performed to investigate the compositional analysis of synthesized $Pr_6O_{11}$ nanorods as shown in Fig. 2a. It is observed that the atomic percentage of each element is same as the stoichiometric ratio of $Pr_6O_{11}$ materials (Pr:O = 0.545:1). The variation in stoichiometric ratio is within the 2% accuracy limit of error. Therefore, the synthesized $Pr_6O_{11}$ nanorods contain only Pr and O elements without other impurity elements as confirmed by XRD result (Fig. 2b). All of the peaks of XRD pattern are perfectly indexed as pure face-centered cubic phase (space group: Fm3 m-225) with calculated lattice constant a = 5.4678 Å, which is consistent with the standard diffraction pattern of $Pr_6O_{11}$ (JCPDS 42-1121). The well-defined XRD peak indicates that

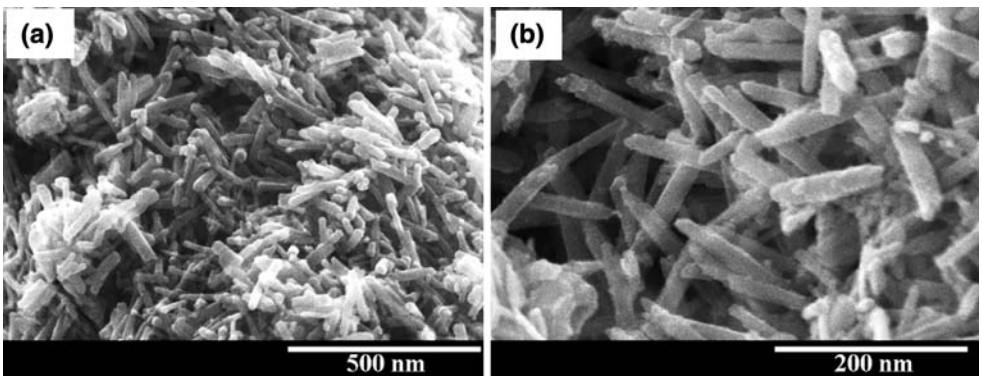


**Fig. 1** **a** low and **b** high magnification FESEM images for $Pr_6O_{11}$ nanorods synthesized at 500°C

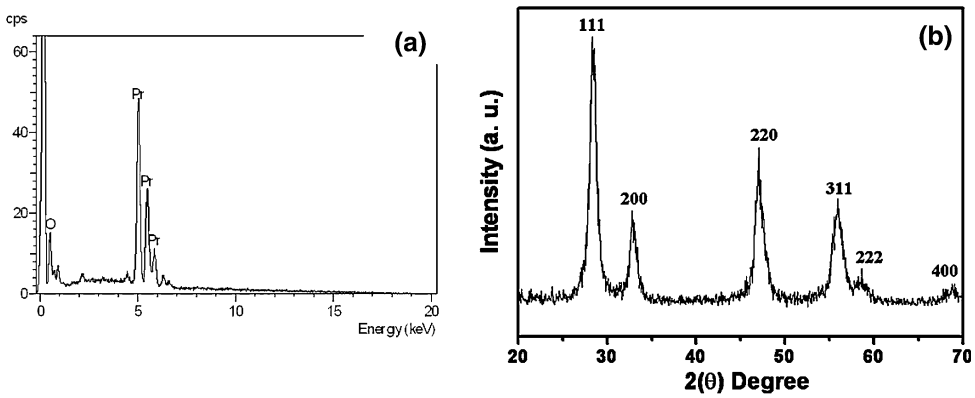


**Fig. 2** **a** EDX spectrum and **b** XRD pattern of $Pr_6O_{11}$ nanorods synthesized at 500°C

$Pr_6O_{11}$ nanorods have good crystalline properties without any impurities.

The morphology of synthesized $Pr_6O_{11}$ nanorods is further examined by transmission electron microscope (TEM, JEOL JEM-2010) and high-resolution TEM (HRTEM) as shown in Fig. 3a and c. The TEM images again affirm that the synthesized $Pr_6O_{11}$ are nanorods morphology with the average diameter of 12–15 nm and length of 100–150 nm. The size of synthesized $Pr_6O_{11}$ nanorods is smaller than that of the reported work [11]. The small size of nanorods may attribute to slow dehydration of $Pr(OH)_3$ during the preparation. Figure 3b exhibits the selected area diffraction (SAED) patterns of a single $Pr_6O_{11}$ nanorod. The SAED pattern of $Pr_6O_{11}$ indexed as a cubic $Pr_6O_{11}$ single crystal, recorded from the [111] zone axis [11]. Figure 3c shows the corresponding HRTEM image with the interplanar distance $d_{111} = 0.313$ nm and is grown along (111) direction. The orientation of the planes and their calculated interplanar distances are consistent with the Fast Fourier Transform (FFT, Fig. 3d) of HRTEM and XRD analysis.

Two major X-ray photoelectron spectroscopy (XPS, AXIS–NOVA, Kratos Inc.) peaks of Pr (Pr 3d) and oxygen (O 1 s) are measured to explain the surface binding between Pr and O atoms as shown in Fig. 4. Pr 3d exhibits the two peaks at 933.2 eV and 953.6 eV (Fig. 4a), which correspond to Pr $3d_{3/2}$ and Pr $3d_{5/2}$ of $Pr_6O_{11}$ nanorods, respectively. It is demonstrated that the peaks at 930 eV and 945 eV in the Pr 3d XPS of $Pr_6O_{11}$ might ascribe to the existence of $Pr^{3+}$ ions in the products [12]. However, Yan et al. reported that the peaks at 933 eV and 954 eV in Pr 3d attributed to Pr $3d_{3/2}$ and Pr $3d_{5/2}$ due to the existence of $Pr^{3+}$ ions in $Pr_6O_{11}$ [11]. Fig. 4b shows the resolved O 1s spectra at 528.1, 530.7 and 532 eV for $Pr_6O_{11}$ nanorods. The lower binding energy (528.1 eV) originated from the oxygen atoms in the lattice [13], and the higher binding energy (531 and 532 eV) can be ascribed to hydroxyl groups on or near the surface of the samples [14]. The relative intensity of lower binding energy (528.1 eV) in O 1s is weaker than those of higher binding energies (531 and 532 eV), indicating the presence of oxygen few deficiency on the surface of $Pr_6O_{11}$ nanorods due to interstitials oxygen chemisorbed on the surface during the synthesis of $Pr_6O_{11}$ nanorods [15]. Atomic ratio of O per Pr on the surface of the praseodymium oxide nanorods is calculated by $\sim 1.86$, which is almost consistent with the theoretical value of $Pr_6O_{11}$ (1.83). It is again confirmed that the synthesized praseodymium oxide $Pr_6O_{11}$ is stable when compared to unstable $PrO_2$ phase, which is in good agreement with XRD results.

Figure 5 shows the conductivity of as grown $Pr_6O_{11}$ nanorods as a function of temperature and the Arrhenius

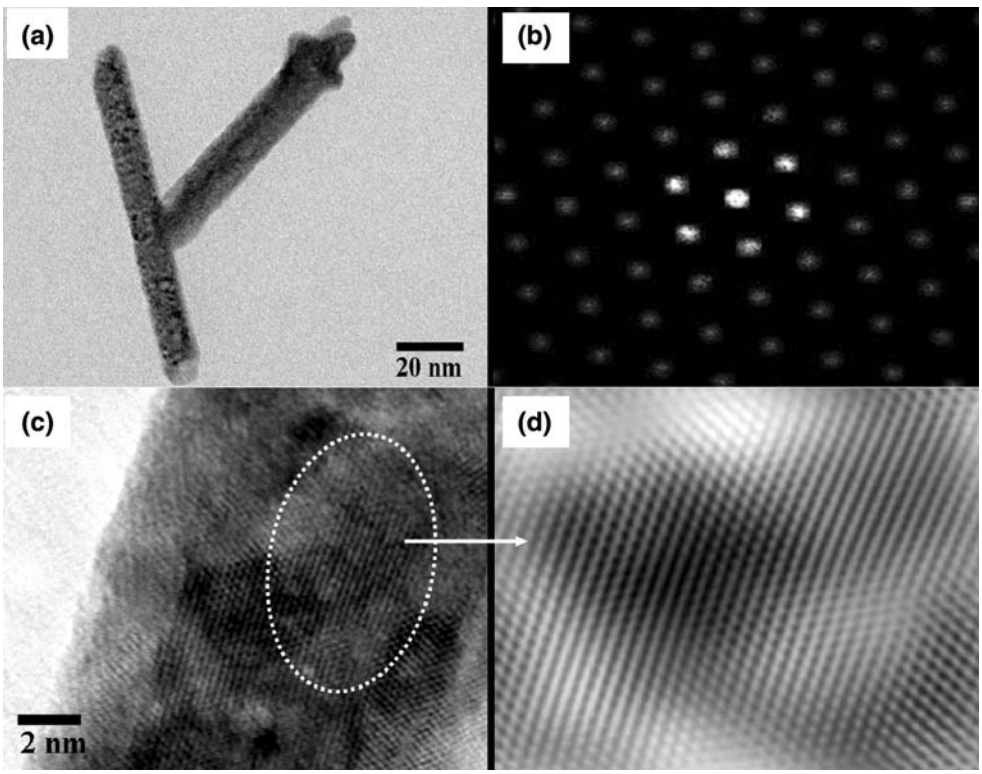


**Fig. 3** **a** TEM image of the $Pr_6O_{11}$ nanorods **b** SAED pattern, **c** HRTEM image of individual $Pr_6O_{11}$ nanorods and **d** Fast Fourier transform (FFT) of HRTEM

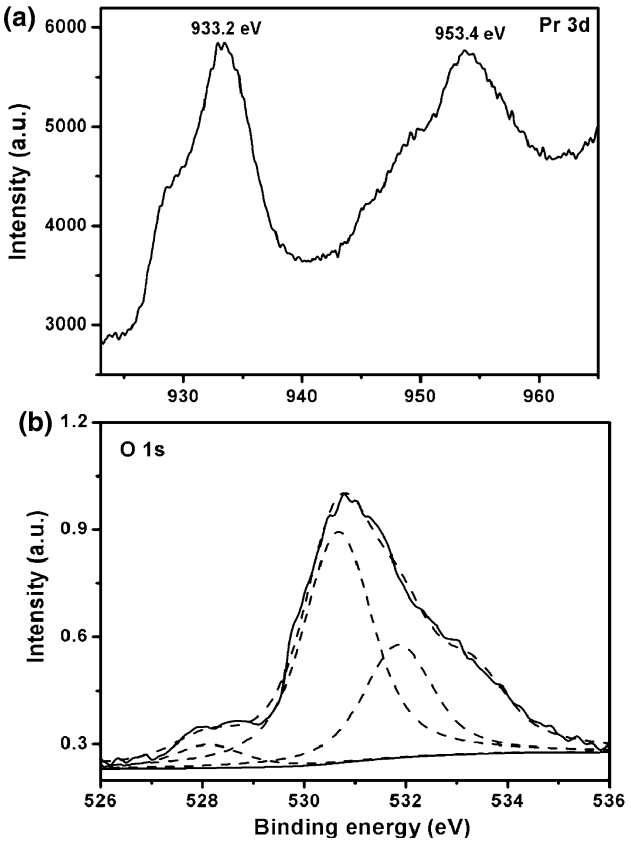


**Fig. 4** XPS spectra of **a** Pr 3d and **b** O 1s of synthesized $Pr_6O_{11}$

plot of ln$\sigma$T vs. 1/T is depicted in inset of Fig. 5, where $\sigma$ is conductivity ($Scm^{-1}$) and T is absolute temperature. The electrical conductivity linearly increases as increasing temperatures from 200° to 850°C. The temperature

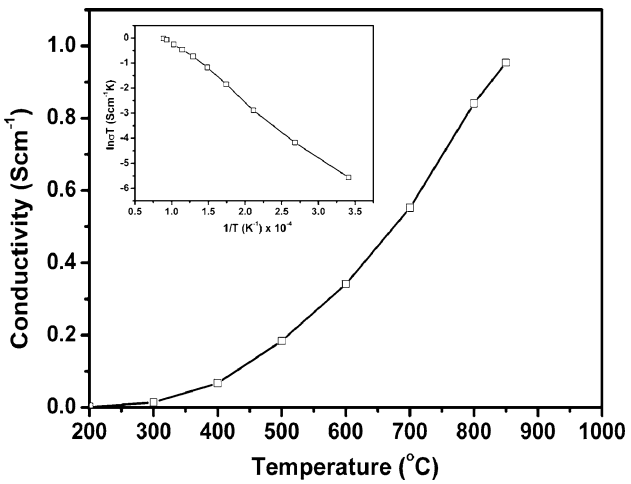


**Fig. 5** The conductivity of synthesized $Pr_6O_{11}$ nanorod as a function of temperature. Inset shows the Arrhenius plot of DC conductivity (ln$\sigma$T) vs 1/T for as prepared $Pr_6O_{11}$ nanorods. The accuracy of obtained conductivities with the larger temperature variation (200–850°C) is to be accurate about ±1% error by measurement system

dependence of the electrical conductivity of $Pr_6O_{11}$ nanorods indicates a typical semiconductor material behavior. The electrical conductivity ($\sigma$) of material seems to be governed by small polaron hopping mechanism as following equation:

$$\sigma = \sigma_0 \exp(-E_a/kT)$$

Where $\sigma_o$ = pre-exponential factor, $E_a$ = activation energy for hopping conduction, $k$ = Boltzmann's constant, $T$ = absolute temperature. The maximum conductivity of as synthesized $Pr_6O_{11}$ nanorods is 0.954 $Scm^{-1}$ at 850°C, which is much higher than those of reported bulk materials $Pr_{0.97}Sr_{0.07}Ga_{0.85}Mg_{0.15}O_3$ (0.1 $Scm^{-1}$ at 850°C) [16]. The activation energy ($E_a$) of electrical conductivity of $Pr_6O_{11}$ nanorods is calculated to be 0.504 eV from the Arrhenius plot as shown in the inset of Fig. 5. Interestingly, $Pr_6O_{11}$ nanorod electrode shows the lower $E_a$ (0.504 eV) when compared to the $Pr_{0.97}Sr_{0.07}Ga_{0.85}Mg_{0.15}O_3$ bulk materials ($E_a$ = 0.88 eV) [16]. It is suggested that synthesized $Pr_6O_{11}$ nanorods constituted the high electronic carriers on the surface of grains upon the removal of chemisorbed oxygen with the increase of temperature, resulting in the high electrical conductivity with low enthalpy [17]. Moreover, the low activation energy of metal oxide supplied the favorable route for charge carrier conduction at high temperature, which leads to the high electronic conductivity [18]. This enhanced electrical conductivity with low activation energy delivers the improved electrochemical properties and high space charge carriers.

To elucidate the charge transport and space charge carrier mobility properties of $Pr_6O_{11}$ nanorod materials, EIS measurements were carried out by applying a 10 mV alternative current (AC) signal over the frequency range of 10–1 MHz. Fig. 6 shows the AC impedance curve of fabricated electrochemical cells by $Pr_6O_{11}$ nanorods in the temperature range of 25–80°C. By the EIS study, it can be demonstrated the charge-transfer across the electrode–electrolyte interface, the order of space charge width in the solid oxide matrix and impedance growth at the surface [19]. As shown in inset of Fig. 6, equivalent circuit can be proposed by consisting of the resistance of electrolyte solution ($R_S$), the charge transfer resistance at the interface of electrolyte and $Pr_6O_{11}$ nanorods ($R_{ct}$), the charge transfer resistance at the interface of $Pr_6O_{11}$ nanorods and FTO ($R_{P/TCO}$), the capacitance of electron accumulation layer in $Pr_6O_{11}$ ($C_{acc}$) and space charge capacitance ($C_{SC}$) [20]. The value of real impedance ($Z_{re}$) at high and low frequencies represents the $R_{P/TCO}$ and $R_{ct}$. The value of $R_{ct}$ at 25°C is estimated approximately ~7285.5 Ω in $Pr_6O_{11}$ nanorods electrodes, which is lower than that of reported value in the order of $10^4$ Ω [2]. While the value of $R_{ct}$ at 80°C decreases to ~4816.2 Ω. The impedance results indicate that $Pr_6O_{11}$ nanorods exhibit the superior electrical

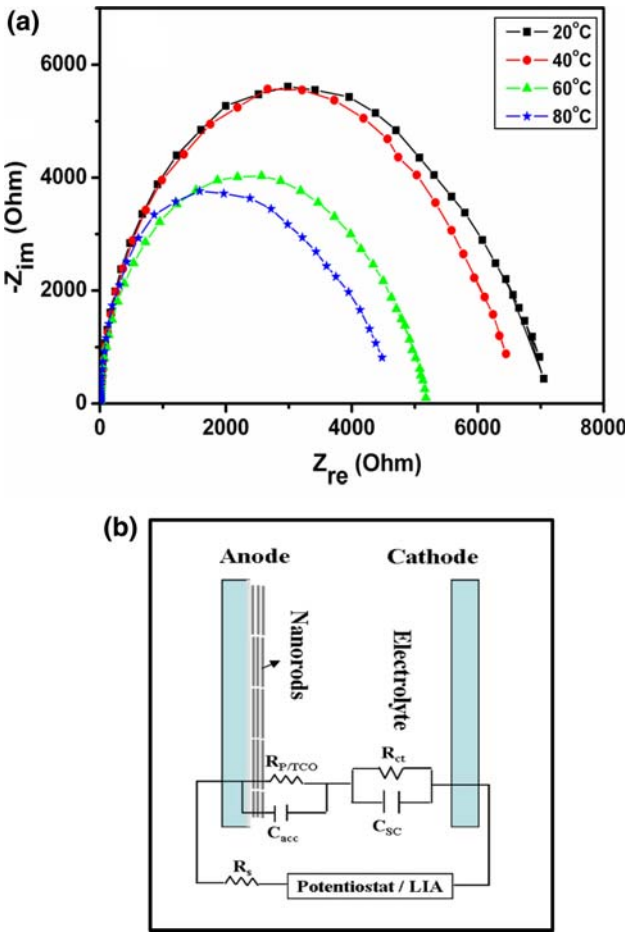


**Fig. 6** **a** Impedance spectra ($Z_{im}$ vs. $Z_{re}$) of synthesized $Pr_6O_{11}$ nanorod as a function of temperature in frequency range of 10–1 MHz and **b** the equivalent circuit of fabricated cells. The accuracy of impedance measurement is probably with the error limit of ±3% by AC impedance analyzer (VersaSTAT 4)

conductivity and high magnitude of space charge width in the nanometric range. The superior electrical conductivity and enlargement of space charge width may attribute to the reduction of grain boundary of synthesized $Pr_6O_{11}$ nanorods [2]. It is known that a small $R_{ct}$ suggests the fast electron transfer in between the electrode to electrolyte interfaces, while a large $R_{ct}$ indicates slow electron transfer in between the electrode to electrolyte interfaces [20]. The impedance (Z) values were dramatically decreased as increasing the temperature in the range of 25°–80°C (Fig. 6). In general, AC impedance of bulk material cells related to their grain size, grain boundaries and electrolyte–electrode interface, which are responsible for high ionic conduction. The decreased resistance at high temperature is due to the reduction of grain boundaries and enlargement of grain sizes, which improves the ionic interaction at electrolyte–electrode interface, resulting in the low $R_{ct}$. Therefore, the low $R_{ct}$ value of synthesized $Pr_6O_{11}$ nanorods is ascribed to the high charge transfer properties within the electrode to electrolyte interface and the reduction in grain boundaries.

## Conclusions

Highly crystalline $Pr_6O_{11}$ nanorods were successfully synthesized by a simple precipitation method. The morphological and crystalline analysis showed that as synthesized $Pr_6O_{11}$ nanorods possess a polycrystalline cubic phase grown in (111) direction with the diameter of 10–15 nm and the length of 100–150 nm. The synthesized $Pr_6O_{11}$ nanorod electrode exhibited the high electrical conductivity with low activation energy and the reduced impedance at high temperature. It is attributed to the reduction of grain boundaries and enlargement of grain size, resulting in the enhanced ionic interaction at electrolyte–electrode interface and low $R_{ct}$. The synthesized $Pr_6O_{11}$ nanorod electrodes would be promising materials for various electrical and sensing devices.

**Acknowledgments** This research is supported by the National Research Foundation (NRF) of Korea through the grant No. R01-2007-000-20810-0 and the Brain Korea 21(BK21) program of the "Center for Future Energy Materials and Devices" in Chonbuk National University. We also wish to thank Korea Basic Science Institute (KBSI) Jeonju branch, and Mr. Jong-Gyun Kang, Centre for University Research Facility (CURF) for performing SEM and TEM images, respectively.



## References

1. H.J. Osten, J.P. Liu, P. Gaworzewski, E. Bugiel, P. Zaumseil, IEDM Technical Digest 653 (2000)
2. S. Shrestha, C.M.Y. Yeung, C. Nunnerley, S.C. Tsang, Sens. Actuators A **136**, 191 (2007)
3. H.J. Mussig, J. Dabrowski, K. Ignatovich, J.P. Liu, V. Zavodinsky, H.J. Osten. Surf. Sci. **504**, 159 (2002)
4. S.C. Tsang, C. Bulpitt, Sens. Actuators B. **52**, 226 (1998)
5. C.F. Qiu, H.Y. Chen, Z.L. Xie, M. Wong, H.S. Kwok, Appl. Phys. Lett. **80**, 3485 (2002)
6. W. Wang, P. Lin, Y. Fu, G. Cao, Catal. Lett. **82**, 19 (2002)
7. U. Chon, J.S. Shim, H.M. Jang, J. Appl. Phys. **93**, 4769 (2003)
8. V. Thangadurai, R.A. Huggins, W. Weppner, J. Solid State Electrochem. **5**, 531 (2001)
9. X. Wang, J. Zhuang, Y.D. Li, Eur. J. Inorg. Chem. 946 (2004)
10. P.X. Huang, F. Wu, B.L. Zhu, G.R. Li, Y.L. Wang, X.P. Gao, H.Y. Zhu, T.Y. Yan, W.P. Huang, S.M. Zhang, D.Y. Song, J. Phys. Chem. B. **110**, 1614 (2006)
11. L. Yan, R. Yu, G. Liu, X. Xing, Scripta Mater. **58**, 707 (2008)
12. C.D. Wagner, W.H. Riggs, L.E. Davis, J.F. Moulder, G.E. Muilinberg, *Handbook of X-ray Photoelectron Spectroscopy* (Perkin–Elmer Corporation, Minnesota, 1973)

13. Y. Zhang, R. Si, C. Liao, C. Yan, J. Phys. Chem. B. **107**, 10159 (2003)
14. A. Laachir, V. Perrichon, A. Badri, J. Lamotte, E. Catherine, J.C. Lavalley, J.E. Fallah, L. Hilaire, F.L. Normand, E. Quemere, G.N. Sauvion, O. Touret, J. Chem. Soc. Faraday Trans. **87**, 1601 (1991)
15. M. Futsuhara, K. Yoshioka, O. Takai, Thin Solid Films **317**, 322 (1998)
16. T. Ishihara, H. Furutani, H. Arikawa, M. Honda, T. Akbay, Y. Takita, J. Electrochem. Soc. **146**, 1643 (1999)
17. A. Tschöpe, J.Y. Ying, H.L. Tuller, Sens. Actuators B: Chem. **31**, 111 (1996)
18. A.K. Vijh, J. Mater. Sci. **9**, 985 (1974)
19. F. Nobili, F. Croce, B. Scrosati, R. Marassi, Chem. Mater. **13**, 1642 (2001)
20. J. Bisquert, J. Phys. Chem. B **106**, 325 (2002)